Nature 2006-05-05564

Supplementary Information

Visualization of transient encounter complexes in protein-protein association

Chun Tang, Junji Iwahara & G. Marius Clore

Laboratory of Chemical Physics, National Institute of Diabetes and Digestive and Kidney Diseases, National Institutes of Health, Bethesda, Maryland 20892-0520, U.S.A.

1. Intramolecular PRE.

The intramolecular PRE data were collected on a sample comprising 0.3 mM U-[^{15}N]-labeled HPr with unlabeled EIN in slight excess. The correlation between observed and back-calculated $^{1}H_N$-Γ_2 rates (80 data points) is shown in Fig. S1. Back-calculation is based on the structure of the stereospecific EIN-HPr complex.[S1] The PRE Q-factor is 0.18 and the correlation coefficient is 0.94.

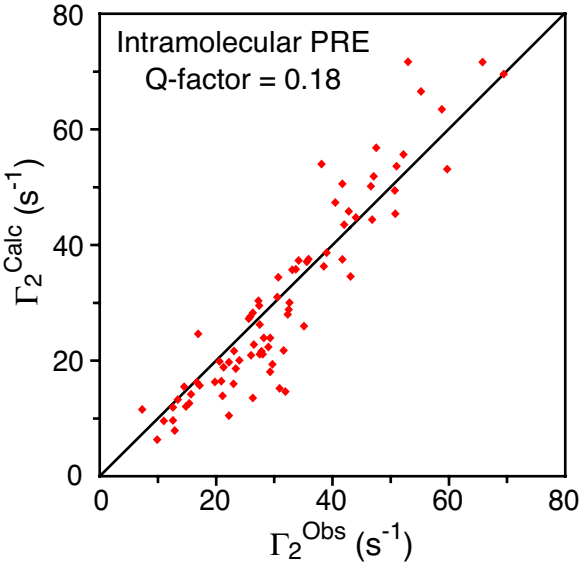

Fig. S1

2. Rate of exchange in the EIN-HPr system

From the maximum chemical shift difference, $\Delta\delta_{max}$, between the free and bound states, and the observation that the linewidths in the bound state are fully consistent with those expected for a ~40 kDa complex, one can deduce that the exchange rate between free and bound states is >5000 s^{-1} (i.e. $>10\pi\Delta\delta_{max}$).[S2] However, in terms of the current experiment, the averaging of the PRE is determined not by exchange between free and bound states but by exchange between the stereospecific complex and the minor species which is likely to be several orders of magnitude faster. Thus, the observed ^1H_N-Γ_2 rates are the weighted average of the contribution of the stereospecific complex and the transient encounter complexes.[S3]

3. Occupancy of non-specific HPr complexes in the vicinity of the specific contact site on EIN.

3.1

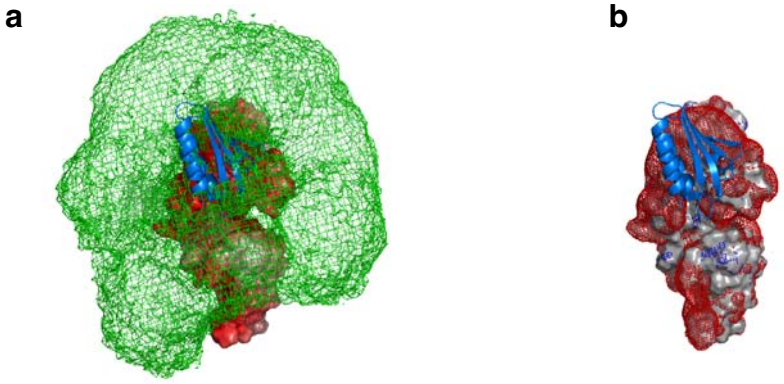

Fig. S2 Distribution of HPr on the surface of EIN in the non-specific encounter complexes derived from the PRE data. a, Reweighted atomic probability map[S4] (computed from 100 calculations with an ensemble size *N*=20) plotted at a threshold of 10% of maximum (green mesh) illustrating the distribution of non-specific HPr encounter complexes on the surface of EIN (color coded by its electrostatic potential, ±8 kT). Occupancy of non-specific HPr complexes in the vicinity of the specific contact site on EIN only becomes fully apparent when the probability density map is plotted at thresholds ≤10% of maximum. **b,** Electrostatic isosurface (blue and red mesh) of EIN plotted at ±7kT reveals that the specific HPr interface on the surface of EIN (grey) does not display the highest negative electrostatic potential. In both panels, HPr in the stereospecific complex is depicted as a blue ribbon diagram.

3.2 Forcing the HPr ensemble to occupy the region of the specific site of EIN.

In control calculations we made use of a 'reduced' radius of gyration (R_{gyr}) term,[S5] applied only to the EIN residues present at the specific interface and the entire HPr molecule to force the HPr molecules within an ensemble (of N = 20) to occupy, in any orientation, the region comprising the specific binding site of EIN. For values of the 'reduced' R_{gyr} force constant ranging from 0.01 to 1 kcal.mol^{-1}.Å^{-2}, the distribution of HPr on the surface of EIN was the same as that reported in the paper and Fig. S2, and the PRE Q-factor is essentially unaffected (Fig. S3a). As the 'reduced' R_{gyr} force constant is increased beyond 1 kcal.mol^{-1}.Å^{-2}, the PRE Q-factor increases dramatically (Fig. S3a) concomitant with the increased occupancy of the specific site of EIN by the HPr ensemble as the 'reduced' R_{gyr} term begins to take effect. At a value of 1000 kcal.mol^{-1}.Å^{-2} for the 'reduced' R_{gyr} force constant all members of the ensemble are located in the region of the specific site on EIN (Fig. S3b) and agreement between observed and calculated PRE values is as poor as that for the stereospecific complex.

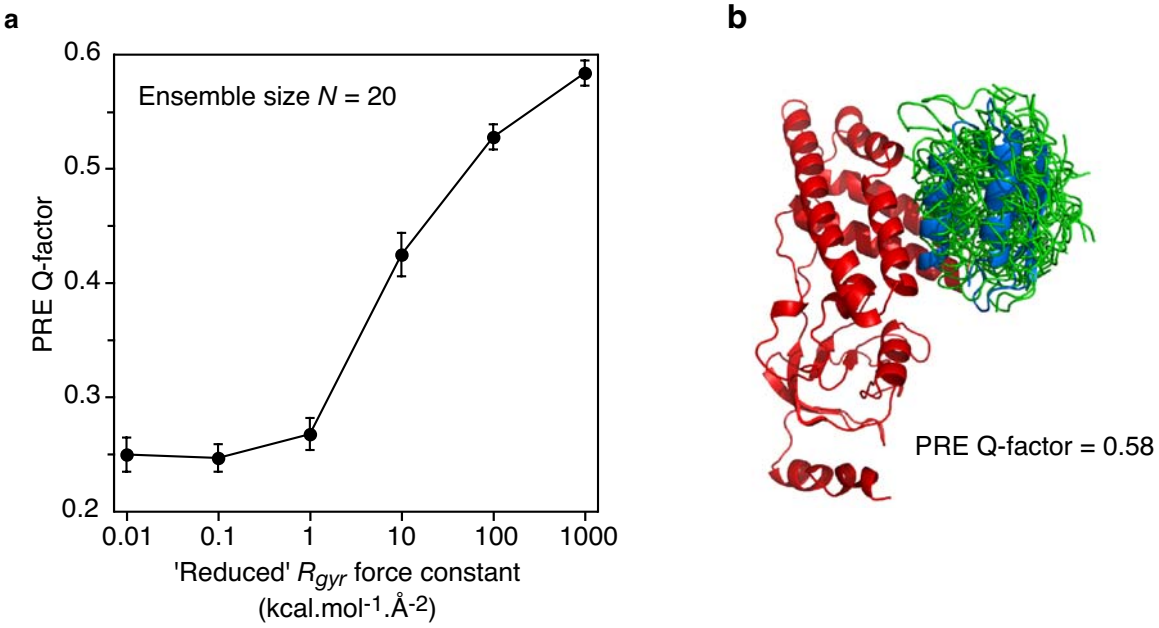

Fig. S3 Dependence of PRE Q-factor on the 'reduced' R_{gyr} force constant. a, Effect of increasing the R_{gyr} force constant from 0.01 to 1000 kcal.mol^{-1}.Å^{-2} with an ensemble size of N=20. **b**, Representative ensemble obtained with a 'reduced' R_{gyr} force constant of 1000 kcal.mol^{-1}.Å^{-2}. EIN and HPr of the stereospecific complex are shown as red and blue ribbons, respectively; the multiple conformers of HPr minor species with a range of orientations and slight translations within the active site of EIN are shown as green tubes.

4. Supplementary views of the distribution of HPr non-specific encounter complexes on the surface of EIN and of the electrostatic isosurface of EIN, together with additional characterization of the nature of the non-specific encounter complexes.

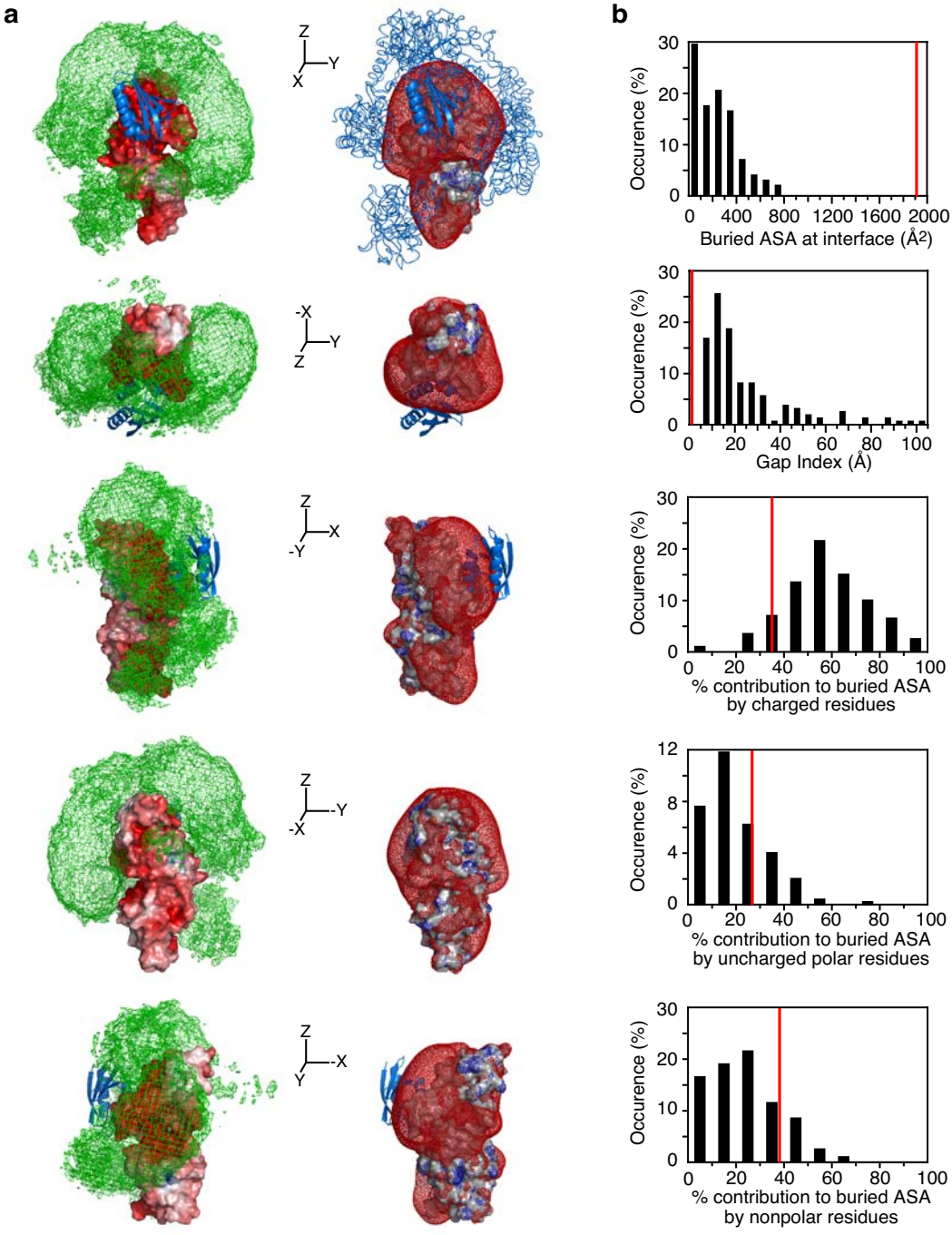

Fig. S4

Fig. S4 Characterization of non-specific EIN-HPr encounter complexes. a, Views illustrating the distribution of HPr on the surface of EIN in the non-specific encounter complexes. In the left-hand panels, the overall distribution of HPr molecules obtained from 100 calculations (ensemble size N=20) is displayed as a reweighted atomic probability density map[S4] (plotted at a threshold of 20% maximum, green) on the molecular surface of EIN (color coded by electrostatic potential, ±8kT). In the right-hand panels the molecular surface of EIN is shown in grey, and the electrostatic potential isosurface of EIN, calculated at ±5kT, is displayed as red (negative) and blue (positive) meshes. The disposition of HPr molecules (shown as blue tubes) in a typical N=20 ensemble is displayed in the top right-hand panel. The location of HPr in the stereospecific complex is shown in all panels as a blue ribbon. Movies representations of the left and right-hand panels of (a) are also provided in additional Supplementary Information. **b,** Histograms of interface buried ASA, gap index, contribution of residue types for the non-specific encounter complexes. Values for the sterospecific complex are indicated by the red lines.

Table S1 Analysis of interfaces in non-specific EIN-HPr encounter complexes

	<Non-specific EIN-HPr encounter complexes>	Stereospecific EIN-HPr complex[a]
Interface ASA (Å^2)[b]	241±177	1945
Gap volume (Å^3)[c]	4586±1230	4085
Gap index (Å)[c]	24.0±19.7	2.1
Planarity (Å)[d]	0.91±0.44	2.7

[a]The values for the specific complex are quite typical of optional (non-obligate) complexes, that is protein-protein complexes where the partners can exist in both the free state and complexed to one another.[S6]

[b]The interface ASA is the sum of the buried ASA at the interface for both partners. Buried interface ASA was calculated using Xplor-NIH.[S7]

[c]Gap volume was calculated using SURFNET.[S8] The gap index is the ratio of the gap volume to the buried ASA at the interface.

[d]Planarity, calculated using SURFNET,[S8] is defined as the atomic rms deviation of all the interface atoms from the least-squares plane through all these atoms. The larger the value, the greater the curvature of the interface.

5. Inverse simulated annealing calculations with an EIN ensemble and HPr fixed

The majority of simulated annealing calculations using ensemble refinement against the intermolecular PRE data were carried out with the structure of the EIN-HPr stereospecific complex held fixed and the positions of the HPr molecules comprising the non-specific encounter complexes (represented by ensembles of varying sizes) allowed to rotate and translate as rigid bodies (see main text). Control calculations were also carried out in which EIN, instead of HPr, was represented as an ensemble of non-specific encounter complexes with the EIN molecules allowed to rotate and translate as rigid bodies. The results of these 'reverse' calculations are essentially identical as summarized in Fig. S5.

Fig. S5 Results of ensemble refinement against the intermolecular PRE data with EIN represented by an ensemble. a, Dependence of the intermolecular PRE Q-factor on the ensemble size of EIN with a population of 10% for the minor species. The average Q-factor, Q_e, for 100 independent calculations is shown in red, and the ensemble of ensembles average Q-factor, Q_{ee}, is shown in blue. The results are essentially identical to those reported in Fig. 2a of the main paper using an HPr ensemble. **b,** Comparison of the distribution of HPr on the surface of EIN in the non-specific encounter complexes derived from 100 calculations using an ensemble (N = 10) of EIN (left-panel) or HPr (right panel) molecules, displayed as a reweighted atomic probability density map (plotted at a threshold of 10% maximum, green) on the molecular surface of EIN (color coded by its electrostatic potential, ±8kT). The location of HPr in the stereopecific complex is shown as a blue ribbon. The representation shown in the left-hand panel is obtained by superimposing EIN from all the non-specific encounter complex structures. **c,** Two views (related by a 180° rotation) comparing the distribution of EIN on the surface of HPr in the non-specific encounter complexes derived from the same two sets of 100 calculations using an ensemble of EIN (left panels) or HPr (right panel) molecules, displayed as a reweighted atomic probability density map (plotted at a threshold of 20% maximum, green) on the molecular surface of HPr (color coded by its electrostatic potential, ±8kT). The location of the α-domain of EIN in the stereospecific complex is shown as a red ribbon. (Note only the α-domain for the stereopecific complex is shown to permit an unobstructed view). The representation shown in the right-hand panel is obtained by superimposing HPr from all the non-specific encounter complex structures.

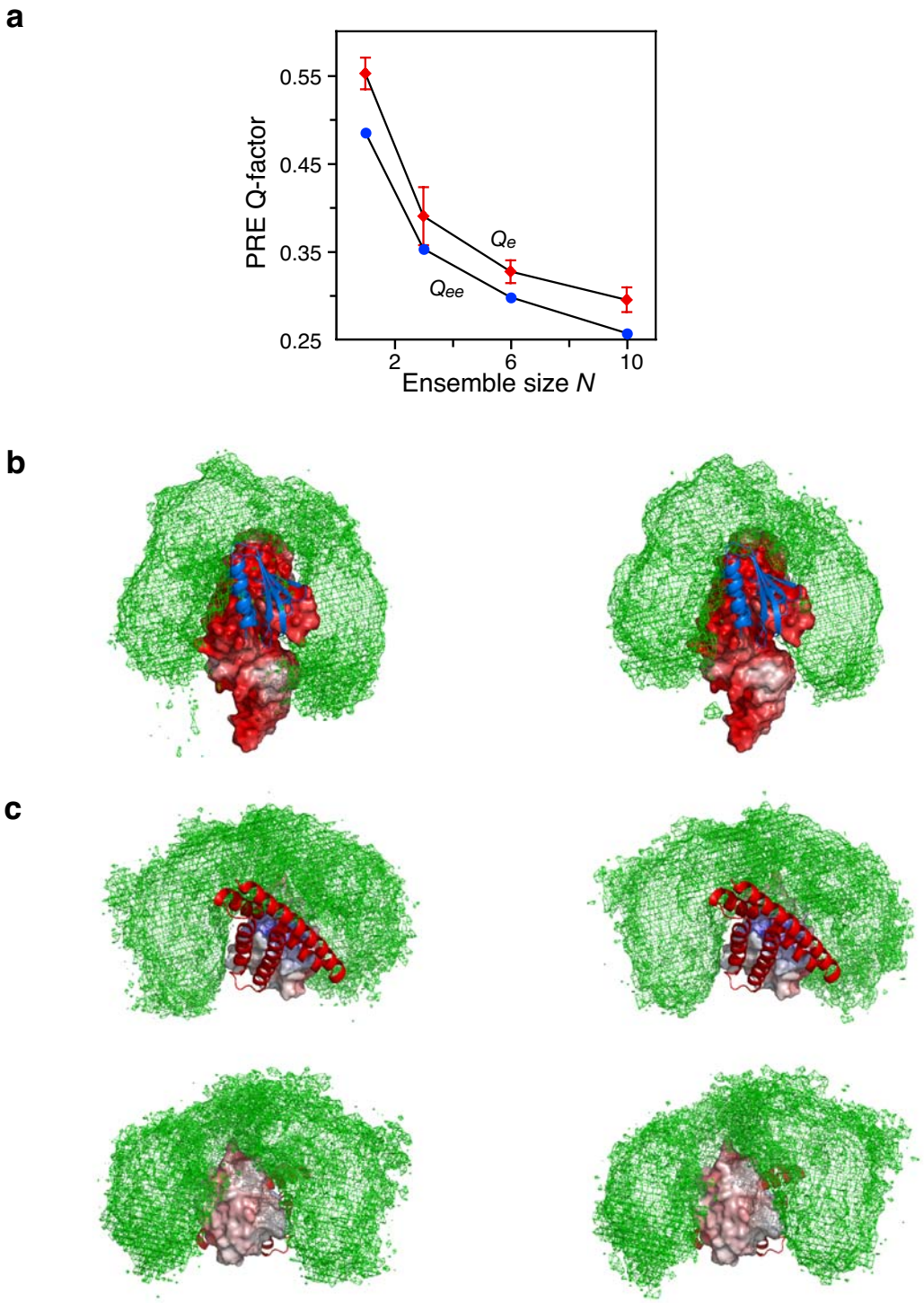
a
0.55
0.45
0.35
0.25
PRE Q-factor
Qe
Qee
2
6
10
Ensemble size N
b
c
Calculations using an EIN ensemble
Calculations using a HPr ensemble

Fig. S5

6. Intermolecular PREs observed for the IIA^{Mannose}-HPr complex with the paramagnetic label on HPr located at E5C

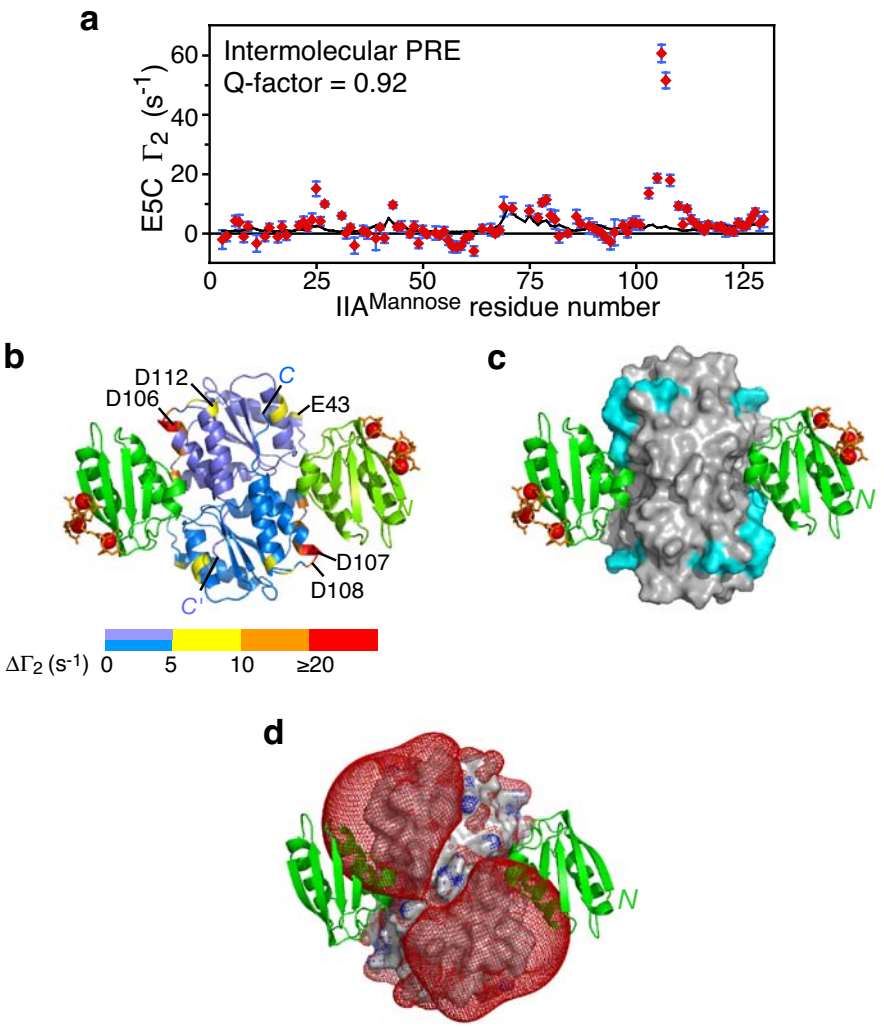

Fig. S6 Observed and calculated PRE $^{1}H_N$-Γ_2 rates for the IIA^{Mannose}-HPr complex obtained with HPr (E5C-EDTA-Mn^{2+}). a, Comparison of intermolecular $^{1}H_N$-Γ_2 rates (red circles) with those back-calculated (black lines) from the structure of the stereospecific complex.[S9] (Error bars: ±1 s.d.). **b,** Structure of the stereospecific complex with the IIA^{Mannose} dimer color coded according to the difference $\Delta\Gamma_2$ between observed and calculated intermolecular $^{1}H_N$-Γ_2 rates. **c**, Molecular surface representation of the IIA^{Mannose} dimer in the stereospecific complex with residues of IIA^{Mannose} exhibiting large $\Delta\Gamma_2$ colored in cyan. **d,** Electrostatic potential isosurface for the IIA^{Mannose} dimer (±5*kT* in blue and red, respectively). In (**c**) and (**d**) HPr is displayed as a green ribbon. The same view is shown in **b-d**.

7. Methods

7.1 Sample preparation. EIN, $IIA^{Mannitol}$, $IIA^{Mannose}$ and HPr were expressed in E. *coli* BL21-star cells (Invitrogen) and grown either in LB-broth or isotope-enriched M9 minimal medium. The proteins were purified by chromatography through the sequential application of DEAE, Superdex-75 and Mono-Q columns, as described previously.[S1,S9,S10] HPr mutant genes (E5C, E25C and E32C) were constructed using QuikChange (Stratagene). During the purification of HPr mutant proteins the reducing agent dithiothreitol (DTT) was always present. DTT was removed by a desalting column prior to incubating the mutant HPr proteins overnight at room temperature with a 5 times excess of N-[S-(2-pyridylthio)cysteaminyl]ethylene-diamine-N,N,N',N'-tetraacetic acid (Toronto Research Chemicals) chelated with divalent cation (Mn^{2+} or Ca^{2+}).[S11] The conjugated protein was further purified with a Mono-Q column. The HPr mutants conjugated with Mn^{2+}-chelated EDTA were confirmed by electro-spray mass spectrometry.

7.2 NMR spectroscopy. Samples comprised ~0.3 mM EIN-HPr complex (with HPr covalently linked to EDTA-Mn^{2+} at E5C, E25C or E32C) in 10mM Tris-HCl buffer (pH 7.4) treated with Chelex-100 (Sigma-Aldrich) to remove any metal ion contaminant. PRE data were acquired at 40°C on a Bruker DRX-600 spectrometer equipped with cryogenic triple resonance probe, as described.[S12] The intramolecular PRE data were collected on a sample comprising U-[^{15}N]-labeled HPr with unlabeled EIN in slight excess, while the intermolecular PRE data employed a sample comprising U-[^{2}H,^{15}N]-labeled EIN with unlabeled HPr in slight excess. Intermolecular PRE data between U-[^{15}N]-labeled $IIA^{Mannitol}$ or $IIA^{Mannose}$ (~0.3 mM) and unlabeled HPr (~0.5 mM and covalently linked to EDTA-Mn^{2+} at E5C) were collected at 35°C using the same buffer conditions given above.

7.3 Back-calculation of intramolecular PREs. Intramolecular PREs for HPr were back-calculated from the structure of the EIN-HPr complex[S1] using a three-conformer ensemble representation for the EDTA-Mn^{2+} groups to account for their flexibility.[S12] The coordinates of the EDTA-Mn^{2+} moieties (with atomic overlap of the EDTA groups permitted) were optimized in torsion angle space by simulated annealing using Xplor-NIH[7] as described previously.[S12] The correlation time τ_c (5.7 ns) used to back-calculate $^{1}H_N$-Γ_2 rates is defined as $(\tau_r^{-1} + \tau_s^{-1})^{-1}$, where τ_r is rotational correlation time of the EIN-HPr complex (14.2 ns determined from backbone ^{15}N T_1 and T_2 relaxation times[S13]) and τ_s the electron relaxation time (9.6 ns for EDTA-Mn^{2+}).[S12]

Ensemble refinement against intermolecular PREs. The following details, in addition to the description in the main text, are relevant. All calculations were carried out using Xplor-NIH.[S7]

The paramagnetic groups on HPr were represented by the three-conformer ensembles obtained from fitting the intramolecular PRE data described above. Random initial starting positions were used for the HPr members of each ensemble. Calculations were carried out using ensemble sizes of N=1, 3, 6, 10 and 20. Simulated annealing involved slow cooling from 1500 K to 25 K with the force constant for the PRE restraints geometrically increased from 0.01 to 1 kcal.mol^{-1}.Hz^{-2}; the force constant for the radius of gyration (R_{gyr}) held fixed at 0.01 kcal.mol^{-1}.Å^{-2} with a target value of 20 Å (calculated from $2.2\alpha^{0.38}$, where α is the total number of ordered residues in the complex[S14]); and the force constant for the van der Waals (vdw) repulsion term increased from 0.004 to 1 kcal.mol^{-1}.Å^{-4} and the vdw radius scale factor decreased from 0.9 to 0.75. Note that the force constant for the R_{gyr} term used here is 10^4 times smaller than that used in structure determination calculations[S14] (and further, increasing the force constant up to a hundred fold had no impact on the results).

References for Supplementary Information

S1. Garrett, D. S., Seok, Y. -J., Peterkofsky, A. , Gronenborn, A. M. & Clore, G. M. Solution structure of the 40,000 M_r phosphoryl transfer complex between the N-terminal domain of enzyme I and HPr. *Nature Struct. Biol.* **6**, 166-173 (1999).

S2. Garrett, D. S., Seok, Y. -J., Peterkofsky, A., Clore, G. M. & Gronenborn, A. M. Identification by NMR of the binding surface of the histidine-containing phosphocarrier protein HPr on the N-terminal domain of enzyme I of the Escherichia coli phosphotransferase system. *Biochemistry* **36**, 4393-4398 (1997).

S3. Iwahara, J. & Clore, G. M. Detecting transient intermediates in macromolecular binding by paramagnetic NMR. *Nature* **440**, 1227-1230.

S4. Schwieters, C. D. & Clore, G. M. Reweighted atomic densities to represent ensembles of NMR structures. *J. Biomol. NMR* **23**, 221-225 (2002).

S5. Tang, C. & Clore, G. M. A simple and reliable approach to docking protein-protein complexes from very sparse NOE-derived intermolecular distance restraints. *J. Biomol. NMR. in press* (2006).

S6. Jones, S. & Thornton, J. M. principles of protein-protein interactions. *Proc. Natl. Acad. Sci. U. S. A.* **93**, 13-20 (1996).

S7. Schwieters, C. D., Kuszewski, J. J., & Clore, G. M. Using Xplor-NIH for NMR molecular structure detemination. *Progr. NMR Spectroscopy* **48**, 47-62 (2006).

S8. Laskowski, R. A. SURFNET: a program for visualizing molecular surfaces, cavities and intermolecular interactions. *J.Mol. Graph.* **13**, 323-330 (1995).

S9. Williams, D. C., Cai, M., Suh, Y. -J., Peterkofsky, A. & Clore, G. M. Solution NMR structure of the 48 kDa $IIA^{Mannose}$-HPr complex of the *Escherichia coli* mannose phosphotransferase system. *J. Biol. Chem.* **280**, 20775-20784 (2005).

S10. Cornilescu, G., Lee, B. R., Cornilescu, C. C., Wang, G., Peterkofsky, A. & Clore, G. M. Solution structure of the phosphoryl transfer complex between the cytoplasmic A domain of the mannitol transporter $II^{Mannitol}$ and HPr of the *Eschrichia coli* phosphotransferase system. *J. Biol. Chem.* **277**, 42289-42298 (2002).

S11. Ebright, Y. W., Chen, Y., Pendergrast, P. S. & Ebright, R. H. Incorporation of an EDTA-metal complex at a rationally selected site within a protein: application to EDTA-iron DNA affinity cleaving with catabolite gene activator protein (CAP) and cro. *Biochemistry* **31**, 10664-10670 (1992).

S12. Iwahara, J., Schwieters, C. D. & Clore, G. M. Ensemble approach for NMR structure refinement against ^{1}H paramagnetic relaxation enhancement data arising from a flexible paramagnetic group attached to a macromolecules. *J. Am. Chem. Soc.* **126**, 5879-5896 (2004).

S13. Clore, G. M., Driscoll, P. C., Wingfield, P. T. & Gronenborn, A. M. Analysis of backbone dynamics of interleukin-1β using two-dimensional inverse detected heteronuclear ^{15}N-^{1}H NMR spectroscopy. *Biochemistry* **29**, 7387-7401 (1990).

S14. Kuszewski, J., Gronenborn, A. M. & Clore, G. M. Improving the packing and accuracy of NMR structures with a pseudopotential for the radius of gyration. *J. Am. Chem. Soc.* **121**, 2337-2338 (1999).